Received: 20 March 2019 | Revised: 28 May 2019 | Accepted: 4 June 2019

DOI: 10.1002/cnr2.1204

ORIGINAL ARTICLE

WILEY Cancer Reports

Tumorigenic effects of *TLX* overexpression in HEK 293T cells

Toshima Z. Parris[1] | Dzeneta Vizlin-Hodzic[2,3] | Susanne Salmela[4] | Keiko Funa[4]

[1] Department of Oncology, Institute of Clinical Sciences, Sahlgrenska Cancer Center, Sahlgrenska Academy at University of Gothenburg, Gothenburg, Sweden

[2] Department of Psychiatry and Neurochemistry, Institute of Neuroscience and Physiology, Sahlgrenska Academy at University of Gothenburg, Gothenburg, Sweden

[3] Department of Physiology, Institute of Neuroscience and Physiology, Sahlgrenska Academy at University of Gothenburg, Gothenburg, Sweden

[4] Department of Medical Biochemistry and Cell Biology, Institute of Biomedicine, Sahlgrenska Cancer Center, Sahlgrenska Academy at University of Gothenburg, Gothenburg, Sweden

Correspondence
Toshima Z. Parris, Department of Oncology, Institute of Clinical Sciences, Sahlgrenska Cancer Center, Sahlgrenska Academy at University of Gothenburg, Gothenburg, Sweden.
Email: toshima.parris@oncology.gu.se

Funding information
Barncancerfonden, Grant/Award Number: 09/001, PROJ07/003 and NBCNSPDHEL11/002; Cancerfonden, Grant/Award Number: 12/386, 09/0669 and 07/0081; Västra Götaland Region/ALF, Grant/Award Number: 76420; Vetenskapsrådet, Grant/Award Number: 2010/2628 and 521-2007-2098; Assar Gabrielsson Research Foundation for Clinical Cancer Research, Grant/Award Number: FB12-94; Swedish Cancer Society, Grant/Award Numbers: 07/0081, 12/386, 09/0669; Swedish Research Council, Grant/Award Numbers: 521-2007-2098 and 2010/2628; ALF (Västra Götaland Region, Sahlgrenska University Hospital, Grant/Award Number: 76420; Swedish Childhood Cancer Fund, Grant/Award Numbers: NBCNSPDHEL11/002, 09/001, PROJ07/003

Abstract

Background: The human orphan receptor TLX (NR2E1) is a key regulator of neurogenesis, adult stem cell maintenance, and tumorigenesis. However, little is known about the genetic and transcriptomic events that occur following *TLX* overexpression in human cell lines.

Aims: Here, we used cytogenetics and RNA sequencing to investigate the effect of *TLX* overexpression with an inducible vector system in the HEK 293T cell line.

Methods and results: Conventional spectral karyotyping was used to identify chromosomal abnormalities, followed by fluorescence in situ hybridization (FISH) analysis on chromosome spreads to assess *TLX* DNA copy number. Illumina paired-end whole transcriptome sequencing was then performed to characterize recurrent genetic variants (single nucleotide polymorphisms (SNPs) and indels), expressed gene fusions, and gene expression profiles. Lastly, flow cytometry was used to analyze cell cycle distribution. Intriguingly, we show that upon transfection with a vector containing the human *TLX* gene (eGFP-hTLX), an isochromosome forms on the long arm of chromosome 6, thereby resulting in DNA gain of the *TLX* locus (6q21) and upregulation of *TLX*. Induction of the eGFP-hTLX vector further increased *TLX* expression levels, leading to G0-G1 cell cycle arrest, genetic aberrations, modulation of gene expression patterns, and crosstalk with other nuclear receptors (AR, ESR1, ESR2, NR1H4, and NR3C2). We identified a 49-gene signature associated with central nervous system (CNS) development and carcinogenesis, in addition to potentially cancer-driving gene fusions (*LARP1-CNOT8* and *NSL1-ZDBF2*) and deleterious genetic variants (frameshift insertions in the *CTSH*, *DBF4*, *POSTN*, and *WDR78* genes).

Conclusion: Taken together, these findings illustrate that TLX may play a pivotal role in tumorigenesis via genomic instability and perturbation of cancer-related processes.

KEYWORDS

cancer, genome instability, NR2E1, nuclear receptors, TLX

1 | INTRODUCTION

The human Nuclear Receptor (NR) superfamily consists of 48 transcription factors that bind to hydrophobic ligands and regulate various physiological processes (eg, development, metabolism, and reproduction) and diseases (eg, cancer).[1,2] NRs are frequently grouped according to their associated ligand, where endocrine NRs bind to steroid hormones, orphan NRs have no known natural ligands, and adopted orphan NRs are associated with ligands that have recently been identified. The NR subfamily 2 group E member 1 (*NR2E1*),

commonly known as *TLX*, is an orphan receptor involved in neurogenesis and adult stem cell maintenance. *TLX* has been shown to be expressed in vertebrate forebrains and the human brain.[3,4] In TLX-mutant mice, the number of retinal cells progressively diminishes, leading to blood vessel malformation.[4-7] In humans and mice, *TLX* represses *PTEN* in the developing retina and the adult brain.[8-11] By controlling *PTEN* expression, *TLX* regulates proliferation of stem cells and cell cycle reentry during retinogenesis.[8,9,11] TLX is also an upstream target of Wnt7a, which binds frizzled receptors, activating the Wnt pathway. In turn, Wnt/β-catenin signaling induces neural stem cell (NSC) self-renewal and proliferation.[12] NSC proliferation is further regulated via TLX-induced expression of Cip/Kip cyclin-dependent kinase inhibitors, namely, $p21^{Cip1}$ (*Cdkn1a*), $p57^{Kip2}$ (*Cdkn1c*), and *p53* downstream target genes.[10,13-18] In fact, *p21* and *p57* are frequently expressed in differentiating neuroprogenitors.[19] Upon TLX-silencing, the nicotinamide adeninedinucleotide (NAD)-dependent deacetylase Sirt1 decreases its protein expression in neuroprogenitors.[20] Thus, TLX regulates the cell cycle, DNA replication, MAPK signaling, and cell adhesion.[21]

Similar to other NRs, eg, estrogen receptor alpha (ERα), androgen receptor (AR), and progesterone receptor (PR), *TLX* has recently been shown to promote cancer stem cell genesis and contribute to cancer development and progression.[1,22-33] Furthermore, *TLX* has emerged as a negative prognostic indicator for multiple malignancies due in part to crosstalk between different NRs.[24,26,28,30] In endocrine cancers, *TLX* expression has been shown to be negatively associated with ERα and AR expression in breast and prostate cancer, respectively. TLX has therefore been proposed to take on the role of ERα and AR in hormone receptor negative cancers.[26] In prostate cancer, TLX has an oncogenic function as its depletion triggered cellular senescence and cell growth arrest, whereas overexpression promoted the aggressive growth of prostate cancer cells.[34] We and others have reported on several molecular mechanisms by which TLX regulates self-renewal of cancer stem cells and tumorigenesis of glioma, neuroblastoma, and glioblastoma.[22,23,25,28,29,31-33] TLX regulates angiogenesis and migration via interaction with *VHL*, *HIF1*, *HIF2*, *MMP2*, and *TLX*-silencing degrades *TGFβ* receptor via interaction with *Smurf1*. Elevated levels of *TGFβ*, inducing epithelial to mesenchymal transduction (EMT), are frequently found in high grade cancers.

Despite strong evidence of the involvement of TLX in tumorigenesis, little is known about genetic aberrations and transcriptional changes associated with TLX overexpression. Here, we investigated the effect of TLX overexpression on genomic instability and transcriptomic changes in HEK 293T cells.

2 | METHODS

2.1 | Cell culture and transfection

The HEK 293T cell line was maintained in Dulbecco's Modified Eagle Medium (DMEM) supplemented with 10% fetal bovine serum (FBS), 100-units/mL penicillin, and 60-μg/mL streptomycin. Cell cultures were monitored for mycoplasma contamination using polymerase chain reaction (PCR) methodology at Sahlgrenska University Hospital, Department of Clinical Microbiology (Gothenburg, Sweden). Human *TLX* (hTLX) cDNA was amplified by PCR (sense, 5′-TAG CGG CCG CTC GAG ATG AGC AAG CCA GCC-3′, antisense, 5′-ATC ATG TCT GGA TCA GAT ATC ACT GGA TTT-3′) and cloned into a pMEP4 inducible vector expressing enhanced green fluorescent protein (pMEP4-eGFP), as previously described.[35] Inserts were verified by Sanger sequencing. Approximately 5×10^4 HEK 293T cells were transfected with the pMEP4-eGFP and pMEP4-eGFP-hTLX vectors using FuGENE transfection reagent (Promega Biotech AB #E2311) according to the manufacturer's recommendations. Stable cell selection was performed by maintaining cultures in 0.3-mg/mL hygromycin B. Monoclonal cell populations were selected by limiting serial dilution. Expression of eGFP or eGFP-hTLX was induced using medium containing 1μM $CdCl_2$ for 22 hours.

2.2 | Immunofluorescence

Immunofluorescence analysis was performed in conjunction with confocal microscopy to compare the intracellular localization pattern of eGFP-hTLX with that of endogenous TLX in HEK 293T cells, as previously described.[36] In brief, 5×10^4 cells were plated on coverslips in 24-well plates and cultured overnight. The cells were fixed with 4.0% paraformaldehyde in phosphate buffered saline (PBS) for 20 minutes, washed three times with 1xPBS for 5 minutes each, permeabilized with 0.25% Triton X-100 in PBS for 5 minutes, and blocked in blocking buffer (0.1% Triton X-100/10% fetal calf serum (FCS)/PBS) for 20 minutes. The slides were incubated for 2 hours with primary anti-GFP (1:1000 dilution, ThermoFisher Scientific #A11122) or anti-TLX (1:100 dilution, R&D #PP-H6506-00) in 0.1% Triton X-100/1% FCS/PBS, followed by three washes with 0.1% Triton X-100/PBS, donkey anti-Rabbit Alexa Fluor 488 (1:1000 dilution, ThermoFisher Scientific #A21206) or donkey anti-Mouse Alexa Fluor 555 (1:1000 dilution, ThermoFisher Scientific #A31570) secondary antibody in 0.1% Triton X-100/1% FCS/PBS for 1 hour, and three final washes with 0.1% Triton X-100/PBS. The nuclei were counterstained with 4′,6-diamidino-2-phenylindole (DAPI) and the coverslips air-dried and mounted. The samples were analyzed using an inverted Zeiss LSM 510 META confocal microscope equipped with a Zeiss image processing system.

2.3 | DNA-protein binding assay

Functionality of the eGFP-hTLX protein was confirmed with pull-down assays using the Oct4 promoter, as previously described.[22,37,38] In brief, biotinylated oligonucleotides (OCT4, 5′-TGA ACC TGA AGT CAG ATT TTT-3′) were diluted in 500-μL 100mM KCl, 10mM Tris-HCl pH 7.4 and incubated with Dynabeads M-280 streptavidin beads (Invitrogen) at room temperature for 30 minutes (1-μL beads/pmol oligonucleotide). The beads were washed three times and incubated for 30 minutes with diluted protein extract from eGFP-hTLX cells in 500-μL binding buffer (100mM KCl, 10mM Tris-

HCl pH 7.4, 0.05% NP-40, 10% Glycerol) followed by six washes in binding buffer. The beads were eluted by boiling in 2 × Laemmli buffer and run on sodium dodecyl sulfate polyacrylamide gel electrophoresis (SDS-PAGE).

2.4 | Flow cytometry-based cell cycle distribution analysis

Cell cycle distribution analyses were performed using harvested eGFP control and eGFP-hTLX HEK 293T cells, fixed with 70% ethanol and stained with propidium iodide/RNase staining solution (Cell Signaling Technology #4087). Data analysis for cell cycle distribution was performed using the FACScalibur system (BD Biosciences). Differences in cell cycle distribution were determined using ANOVA ($P < .05$). Stacked bar plots were created in R/Bioconductor (3.4.3) using the ggplot2 package (3.1.0).

2.5 | FISH and SKY

Probe labeling and hybridization were performed as described elsewhere[39] using locus-specific bacterial artificial chromosome (BAC; BACPAC Resources Center) probes. Three BAC clones (RP11-144P8, RP11-815N24, and RP11-1005B20) spanning the *NR2E1*, *SNX3*, and *OSTM1* genes were pooled and labeled using dioxigenin-11-dUTP. Dual-color fluorescence in situ hybridization (FISH) was performed using the dioxigenin-11-dUTP labeled probe cohybridized with the XCP 6 green whole chromosome painting (WCP) probe for human chromosome 6 (MetaSystems #D-0306-100-FI), followed by counterstaining of the mitotic chromosome spreads with DAPI. The samples were analyzed using a Leica DMRA2 fluorescent microscope (Leica) equipped with an ORCA Hamamatsu charged-couple devices (CCD) camera and filter cubes specific for red rhodamine, green fluorescein isothiocyanate (FITC), and UV for DAPI visualization. Digitalized black and white images were acquired using the Leica CW4000 software package. Conventional spectral karyotyping (SKY) was performed according to standard protocols.

2.6 | RNA sequencing

Total RNA samples from eGFP control and eGFP-hTLX HEK 293T cells were isolated using the Total RNA Purification Plus Kit (Norgen Biotek Corp. #48400), including DNase I treatment to remove genomic DNA contamination. RNA integrity was measured with the Agilent 2100 Bioanalyzer (Agilent Technologies) and RNA concentration using the Nanodrop (ThermoFisher Scientific) and QuBit (ThermoFisher Scientific). RNA integrity number (RIN) values above 8.0 were accepted for further downstream analysis. The RNA samples were stored at −80°C and processed at the Science for Life Laboratory (National Genomics Infrastructure Stockholm) to construct Illumina TruSeq strand-specific RNA libraries (Ribosomal depletion using RiboZero human) with 125 BP pair-end reads on a HiSeq2000 sequencer (Illumina). FASTQ files for two wild type HEK 293T samples (ArrayExpress, accession number E-MTAB-3102) were used as reference.40 Quality control and processing (fusion gene detection and variant calling/filtering) of mapped RNA-sequencing (RNA-seq) reads were performed as previously described.[41] Read alignment yielded approximately 60 million aligned reads per sample. Calculation of Counts and Fragments Per Kilobase of transcript per Million mapped reads (FPKM) was performed using HtSeq (0.6.1) and Cufflinks (2.1.1), respectively. Mapping statistics were generated with RNA-seq Quality Control package (RSeQC). Mapped RNA-seq reads were used to quantify gene-level, transcript-level, and noncoding RNA expression using Cuffmerge, followed by Cuffdiff (Benjamini-Hochberg adjusted P value < .05). Fusion genes and genetic variants were visualized for each sample using the Circos module (0.66). The computations were performed on resources provided by Swedish National Infrastructure for Computing (SNIC) through Uppsala Multidisciplinary Center for Advanced Computational Science (UPPMAX)[42] under Project b2015014.

2.7 | Quantitative real-time PCR

Total RNA was reverse transcribed into cDNA using iScript Reverse Transcription Supermix for RT-quantitative real-time PCR (qPCR) kit (Bio-Rad Laboratories #1708840), followed by qPCR analysis (in triplicate) using SsoAdvanced Universal SYBR Green Supermix (Bio-Rad Laboratories #1725270) and the ddCt method. In brief, total RNA samples for eGFP control (induced and noninduced) and eGFP-hTLX (induced and noninduced) HEK 293T cells were used to validate the expression patterns of *GFP* (sense, 5′-ATC ATG GCC GAC AAG CAG AAG AA-3′, antisense, 5′-GTA CAG CTC GTC CAT GCC GAG AG-3′), *TLX* (sense, 5′-GAT TTA GAC AAC TCC GGT TAG AT-3′, antisense, 5′-TGA AGG GCT GCA ATG GCG GCA GC-3′), *TP53* (sense, 5′-CGG TGA CAC GCT GGA T-3′, antisense, 5′-TTG GGA CGG CGG GAC A-3′), and two endogenous controls (*TBP2* (sense, 5′-ACC CTT GCC GCC ACT C-3′, antisense, 5′-CGG GCA CGA ATG GTC T-3′) and *GAPDH* (sense, 5′-GAA GGT GAA GGT CGG AGT-3′, antisense, 5′-GAA GAT GGT GAT GGG ATT TC-3′). Dissociation curve analysis confirmed the presence of a single amplicon. Normalization and data analysis were performed in GenEx 6.1 (TATAA Biocenter), as previously described.[43]

2.8 | Gene ontology enrichment and IPA

Gene ontology (GO) enrichment analysis was performed using PANTHER Overrepresentation Test (release 20160715) and GO ontology database released 2016-11-30 with Bonferroni correction for multiple testing.[44,45] Canonical pathways and diseases and bio functions analyses were generated for TLX overexpression with Ingenuity Pathway Analysis (IPA; Qiagen, Ingenuity Systems) using Fisher's exact test ($P < 0.05$).

3 | RESULTS

3.1 | *TLX* overexpression perturbs cell cycle progression in HEK 293T cells

Full-length recombinant hTLX was stably expressed in HEK 293T cells using the pMEP4 inducible system with $CdCl_2$. Functionality of the eGFP-hTLX protein was confirmed with DNA pull-down assays using the Oct4 promoter (Figure 1A). Although limiting serial dilution was used to produce a stable monoclonal population, evaluation of GFP expression with confocal microscopy revealed the presence of polyclonal colonies containing populations that were resistant to hygromycin B but with variable expression of GFP and nuclear localization of eGFP-hTLX (Figure 1B). In comparison with their noninduced counterparts, GFP and *TLX* mRNA levels were both found to be elevated in induced eGFP controls and eGFP-hTLX cells using qPCR analysis (Figure 1C). Additionally, RNA-seq analysis confirmed the presence of the Simian virus 40T (SV40 T) antigen in the HEK 293T cells and overexpression of the *TLX* gene (*NR2E1*) in induced eGFP-hTLX cells (FPKM value 34.7 vs 0.7 in induced eGFP-hTLX and eGFP control cells, respectively). As is characteristic of the HEK 293 cell line and its derivatives, SKY demonstrated genomic rearrangements on the telomeric end of chromosome 1q.[46] In line with previous studies, *TLX* overexpression was shown to perturb cell cycle progression and repress the expression levels of cell cycle inhibitors such as *CDKN1A*/p21 and *PTEN* by 40% and 39%, respectively. Evaluation of cell cycle progression revealed an accumulation of *TLX*-overexpressing cells in G0-G1 phase and a decrease in the number of cells in S phase (Figure 2). Consequently, decreased *CCNE1* and *CCNE2* expression levels (FPKM value 19.5 vs 22.1 for *CCNE1* and 13.6 vs 20.4 for *CCNE2* in induced eGFP-hTLX and eGFP control cells, respectively) were observed that are commonly elevated during G1-S transition, indicating cell cycle arrest at the G0-G1 phase following *TLX* overexpression.

3.2 | Isochromosome 6q formation in eGFP-hTLX HEK 293T cells

DNA copy number analysis was then performed using dual-color FISH with a locus-specific probe for the *TLX* gene cohybridized with a chromosome-specific WCP probe for chromosome 6. Both induced and noninduced eGFP control cells frequently displayed disomy or trisomy for chromosome 6 with normal DNA copy numbers of the *TLX* gene on each chromosome. In contrast, eGFP-hTLX expressing cells (induced and non-induced) showed extensive copy number heterogeneity, ie, cell populations with trisomy or tetrasomy chromosome 6 with normal *TLX* copy numbers and other cell populations with one to three chromosome 6 (normal *TLX* copy numbers) and one monocentric isochromosome of the long arm of chromosome 6 [i(6q)](Figure S1). Each i(6q) contained four FISH signals for the *TLX*-specific probe with two signals on each chromosome arm. Furthermore, both wild type chromosome 6 and i(6q) were shown to be homogeneously stained along the entire chromosome with the WCP probe indicating the absence of contributing genetic material from

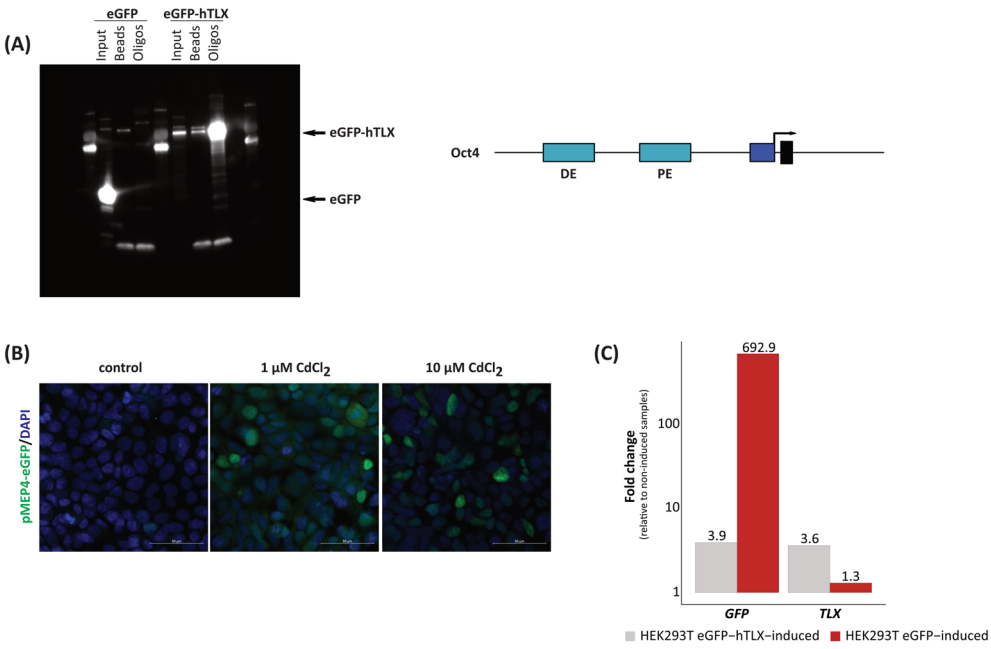

FIGURE 1 Detection of active *TLX* in HEK 293T cells. A, DNA pull-down assays using Oct4 promoter showed that expressed eGFP-hTLX binds to DNA. Schematic diagram showing the distal enhancer (DE) and proximal enhancer (PE) of Oct4. B, Green fluorescent protein (GFP) expression was monitored in noninduced (control) and induced (1 or 10µM $CdCl_2$) eGFP-hTLX HEK 293T cells using confocal microscopy (40X). Nuclei were counterstained using 4′,6-diamidino-2-phenylindole (DAPI). Scale bar, 50 µm. C, Quantitative real-time PCR analysis demonstrated elevated *GFP* expression levels in induced eGFP and eGFP-hTLX HEK 293T cells, and elevated *TLX* expression levels in eGFP-hTLX cells. Relative fold change was estimated by the delta Ct method

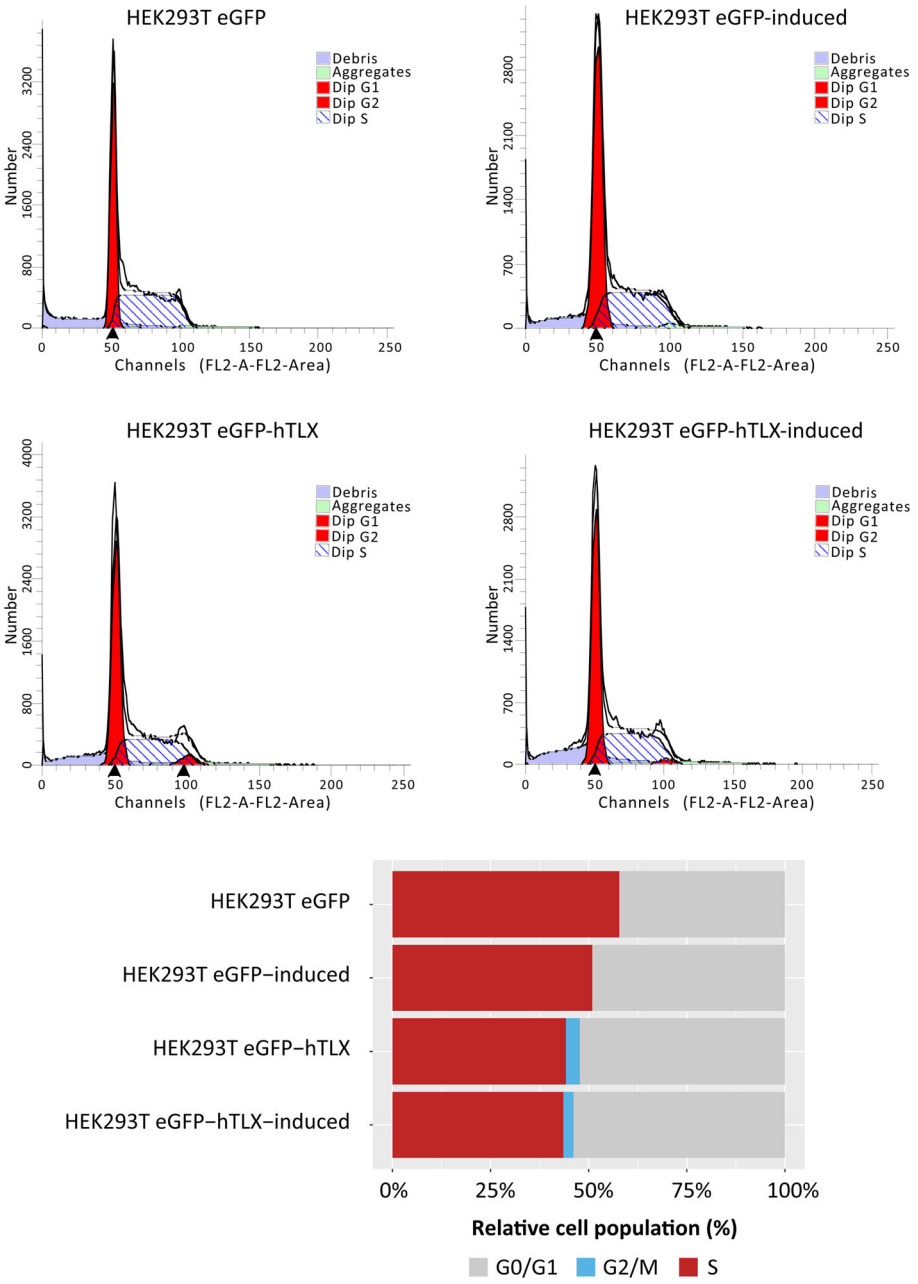

FIGURE 2 *TLX* overexpression results in accumulation of cells in G0/G1. Cell cycle distribution analysis was performed for eGFP and eGFP-hTLX HEK 293T cells (before and after induction with $CdCl_2$) with flow cytometry. Representative DNA histograms and stacked bar charts show the distribution of cell populations in each cell cycle phase. The data are presented for three independent experiments

other chromosomes (Figure 3). Quantitative PCR demonstrated a 16- and 44-fold increase in *TLX* expression in noninduced and induced eGFP-hTLX cells compared with eGFP controls, respectively.

3.3 | *TLX* overexpression is associated with CNS development and tumorigenesis

To assess the effect of *TLX* overexpression in HEK 293 T cells, RNA-seq analysis was performed to evaluate changes in gene expression, genetic variants, and structural rearrangements in induced eGFP control and *TLX*-overexpressing cells. In total, a gene signature containing 49 differentially expressed transcripts (*P* adjusted value < .05) was identified, of which 16 transcripts were downregulated and 33 were upregulated in *TLX*-overexpressing cells compared with controls (Table 1). GO enrichment analysis showed an association between nine of the 49 differentially expressed transcripts (*NR2E1/TLX*, *GPR56*, *CA10*, *PCDH19*, *NMUR2*, *SEPP1*, *SLC7A11*, *GHRHR*, and *CXCL12*) and central nervous system (CNS) development (GO:0007417; 6.61 fold enrichment, 4.22E-02). Further analysis of the eGFP-hTLX-enriched transcripts with IPA showed an association with several cellular stress responses, ie, cell death and survival, carbohydrate metabolism, cellular function and maintenance, cellular movement, and cell cycle. Pathway analysis identified a number of

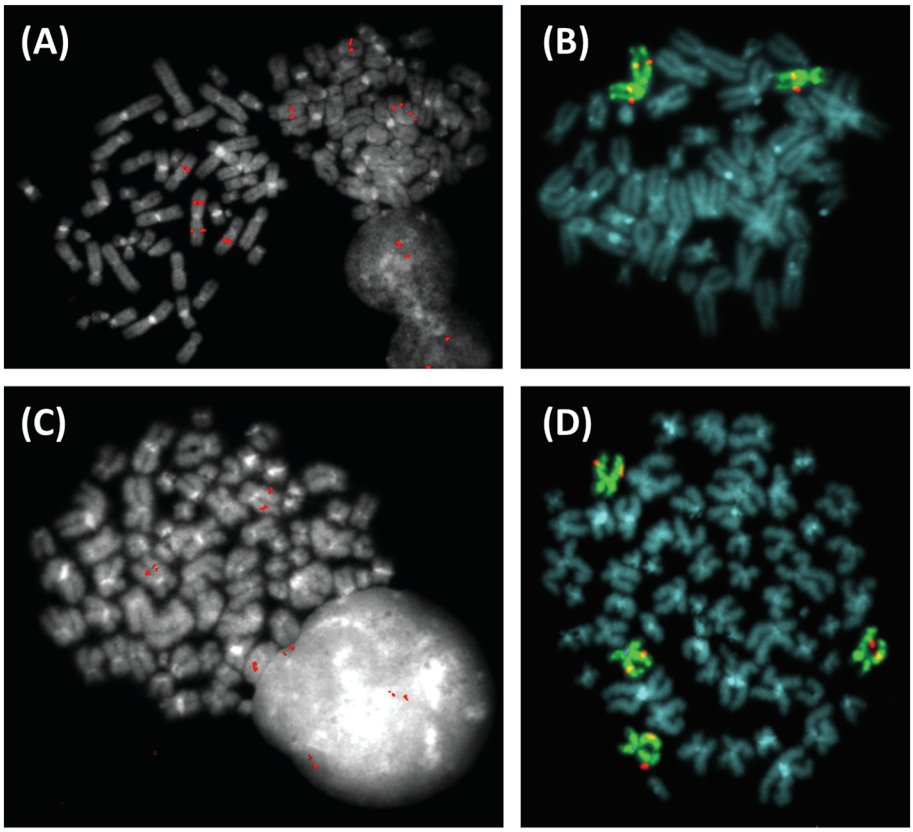

FIGURE 3 FISH analysis of a *TLX*-specific probe in eGFP control and eGFP-hTLX HEK 293T cells. A-B, eGFP-hTLX cells showing an isochromosome 6 [i(6q)], with four hybridization signals for the *TLX*-specific probe in each cell. C-D, eGFP control cells with normal chromosome 6. Digoxigenin-11-dUTP labeled probe (red) containing the RP11-144P8, RP11-815 N24, and RP11-1005B20 BAC clones spanning the *NR2E1*, *SNX3*, and *OSTM1* genes. Metaphase spreads were counterstained using 4′,6-diamidino-2-phenylindole (DAPI). B and D show homogeneous staining for chromosome 6 using a chromosome-specific whole chromosome painting probe (green)

significantly affected canonical signaling pathways and predicted upstream regulators such as AR ($P < .05$), including an association with the molecular mechanisms of cancer and chemokine signaling (Table 2). No differentially expressed isoforms, coding DNA sequence, or transcription start site groups were identified.

3.4 | TLX-overexpressing cells harbor potential driver fusion genes

The RNA-seq paired-end reads were then used to identify candidate somatic fusion genes. In total, 46 fusion genes (63 fusion transcripts) and 48 fusion genes (73 fusion transcripts) were identified in eGFP and eGFP-hTLX cells, respectively (Table S1). Few recurrent fusion genes (*RPPH1-XIST*, *XIST-GNB2L1*, and *XIST-RBBP7*) were detected in both transfected cell lines (Figure 4), and a comparatively high proportion of the fusion transcripts found in eGFP controls spanned at least one noncoding gene partner (95% in controls compared with 89% in *TLX*-overexpressing cells). Additionally, gene fusions with potential functional activity were identified in *TLX*-overexpressing cells, including promoter-coding (5′UTR; *NDUFC2-ALG8* and *NSL1-ZDBF2*), coding-3′UTR (*COPB1-PSMA1*), and in-frame/coding-coding fusions (*COPB1-PSMA1* and *LARP1-CNOT8*). Functional protein domains were found in the *NDUFC2-ALG8* (GVQW domain), *COPB1-PSMA1* (proteasome domain) and *LARP1-CNOT8* (LA and DM15 domains) fusions using the Simple Modular Architecture Research Tool (SMART) online tool (Figure 5). The Oncofuse Bayesian classifier pipeline was then used to identify driver fusion genes with oncogenic potential (putative oncofusions). In *TLX*-overexpressing cells, *LARP1-CNOT8* and *NSL1-ZDBF2* were classified as putative oncofusions, whereas no driver fusions were found in the eGFP controls. Interestingly, one or both of the gene fusions partners for *NDUFC2-ALG8* and *LARP1-CNOT8* exhibited elevated expression patterns in eGFP-hTLX cells.

3.5 | Potentially deleterious genetic variants have an impact on gene expression following *TLX* overexpression

Lastly, the GATK variant calling pipeline was used to identify insertions/deletions (indels) and single-nucleotide variants (SNVs) in genomic and exonic (coding) regions. The genetic variants were then filtered to remove variants found in the wild type HEK 293T samples and common genetic variants present in the human population with the dbSNP, 1000 Genomes Project, SweGen dataset, and NHLBI GO

TABLE 1 Differentially expressed transcripts in *TLX* (gene alias NR2E1) overexpressed cells

Gene Symbol	Locus	Sample_1	Sample_2	FPKM value_1	FPKM Value_2	Log2(fold_change)	*P* value	Q-value
TXNIP	chr1:145438468-145442635	eGFP control	eGFP-hTLX	88.0987	22.0705	−1.997	5.00E-05	0.026291
ESRRG	chr1:216676587-217311097	eGFP control	eGFP-hTLX	4.17E-05	0.382267	13.1634	5.00E-05	0.026291
AC074093.1	chr2:145425533-145940216	eGFP control	eGFP-hTLX	0.0111084	0.304505	4.77675	5.00E-05	0.026291
AC079779.5	chr2:305110-314367	eGFP control	eGFP-hTLX	0	0.294624		5.00E-05	0.026291
AMTN	chr4:71384256-71398459	eGFP control	eGFP-hTLX	0	1.30086		5.00E-05	0.026291
BMP3	chr4:81952118-81979101	eGFP control	eGFP-hTLX	5.48225	1.00808	−2.44316	5.00E-05	0.026291
SLC7A11	chr4:138948575-139163547	eGFP control	eGFP-hTLX	8.48423	1.53522	−2.46634	5.00E-05	0.026291
DOCK2	chr5:169064250-169510386	eGFP control	eGFP-hTLX	0.00126699	0.312403	7.94586	0.0001	0.046143
SEPP1	chr5:42756902-42887494	eGFP control	eGFP-hTLX	126.994	34.7852	−1.86822	5.00E-05	0.026291
NMUR2	chr5:151771092-151812929	eGFP control	eGFP-hTLX	0	1.23084		5.00E-05	0.026291
NR2E1	chr6:108487261-108510013	eGFP control	eGFP-hTLX	0.676348	34.6862	5.68045	5.00E-05	0.026291
RNA5SP215	chr6:120783657-121029044	eGFP control	eGFP-hTLX	0	0.735492		5.00E-05	0.026291
HIST1H1A	chr6:26017259-26018040	eGFP control	eGFP-hTLX	2.11128	0		5.00E-05	0.026291
HIST1H2AJ	chr6:27782111-27782607	eGFP control	eGFP-hTLX	10.9604	0		5.00E-05	0.026291
-	chr6:27205140-27206258	eGFP control	eGFP-hTLX	0	1.07429		5.00E-05	0.026291
GHRHR	chr7:30978283-31032869	eGFP control	eGFP-hTLX	0	0.26321		5.00E-05	0.026291
RP5-884M6.1	chr7:106415456-106478563	eGFP control	eGFP-hTLX	0	0.604472		5.00E-05	0.026291
AKR1B10	chr7:134200824-134226160	eGFP control	eGFP-hTLX	0	1.63564		5.00E-05	0.026291
RP11-109M17.2	chr9:10948371-11065013	eGFP control	eGFP-hTLX	0	7.63869		5.00E-05	0.026291
CXCL12	chr10:44793037-44881941	eGFP control	eGFP-hTLX	8.38771	0.81423	−3.36477	0.0001	0.046143
RP11-442H21.2	chr10:74033677-74035794	eGFP control	eGFP-hTLX	44.8117	6.38561	−2.81098	0.0001	0.046143
TMPRSS4	chr11:117886486-117992605	eGFP control	eGFP-hTLX	0	0.564901		5.00E-05	0.026291
PDE2A	chr11:72287184-72385635	eGFP control	eGFP-hTLX	0.0102288	0.693687	6.08357	0.0001	0.046143
-	chr11:26966635-26969518	eGFP control	eGFP-hTLX	0	0.310244		5.00E-05	0.026291
FZD10	chr12:130647003-130650285	eGFP control	eGFP-hTLX	0	0.658753		5.00E-05	0.026291
SCNN1A	chr12:6456008-6500740	eGFP control	eGFP-hTLX	0.00688833	0.375269	5.76763	5.00E-05	0.026291
RP11-143E21.7	chr12:130634631-130646801	eGFP control	eGFP-hTLX	0	1.16637		5.00E-05	0.026291
-	chr13:64667350-64668499	eGFP control	eGFP-hTLX	0.635623	0		0.0001	0.046143
SNRPN,SNURF	chr15:25068793-25684128	eGFP control	eGFP-hTLX	4.04547	0.0343245	−6.88093	5.00E-05	0.026291
GPR56	chr16:57644563-57698944	eGFP control	eGFP-hTLX	0.0544052	0.267494	2.29769	5.00E-05	0.026291
CA10	chr17:49707673-50237377	eGFP control	eGFP-hTLX	0.00119929	2.35606	10.94	5.00E-05	0.026291
-	chr17:13566213-13567322	eGFP control	eGFP-hTLX	0.894106	0		5.00E-05	0.026291
PMAIP1	chr18:57567179-57571538	eGFP control	eGFP-hTLX	457.113	78.4466	−2.54277	5.00E-05	0.026291
C18orf32,RPL17,RPL17-C18orf32	chr18:47008027-47018906	eGFP control	eGFP-hTLX	328.891	98.5848	−1.73817	5.00E-05	0.026291
NARS	chr18:55267887-55289445	eGFP control	eGFP-hTLX	125.23	37.8648	−1.72565	5.00E-05	0.026291
LMAN1	chr18:56995054-57027194	eGFP control	eGFP-hTLX	59.019	19.3265	−1.6106	5.00E-05	0.026291
TMX3	chr18:66340924-66722426	eGFP control	eGFP-hTLX	36.7847	10.2731	−1.84023	5.00E-05	0.026291
ZNF578	chr19:52956828-53015595	eGFP control	eGFP-hTLX	0	0.288237		5.00E-05	0.026291
ZNF701,ZNF808	chr19:53030904-53090427	eGFP control	eGFP-hTLX	0.599326	6.15164	3.35956	0.0001	0.046143
ZNF28,ZNF468	chr19:53300661-53360902	eGFP control	eGFP-hTLX	2.69473	18.8691	2.80781	5.00E-05	0.026291
ZNF321P,ZNF816	chr19:53430387-53541151	eGFP control	eGFP-hTLX	0.0455898	6.06771	7.0563	5.00E-05	0.026291
ZNF347,ZNF415	chr19:53611131-53662328	eGFP control	eGFP-hTLX	0.0407103	0.659815	4.0186	5.00E-05	0.026291

(Continues)

TABLE 1 (Continued)

Gene Symbol	Locus	Sample_1	Sample_2	FPKM value_1	FPKM Value_2	Log2(fold_change)	*P* value	Q-value
PXMP4	chr20:32293442-32308125	eGFP control	eGFP-hTLX	0	0.985993		5.00E-05	0.026291
-	chr21:9831754-9836006	eGFP control	eGFP-hTLX	0	1.05531		5.00E-05	0.026291
FAM19A5	chr22:48885271-49246724	eGFP control	eGFP-hTLX	0	0.621042		5.00E-05	0.026291
ZCCHC12	chrX:117957752-117960942	eGFP control	eGFP-hTLX	11.6004	43.2134	1.89731	5.00E-05	0.026291
PCDH19	chrX:99546641-99665271	eGFP control	eGFP-hTLX	0.631976	8.69655	3.7825	5.00E-05	0.026291
NXF3	chrX:102330737-102348157	eGFP control	eGFP-hTLX	0	0.365767		5.00E-05	0.026291
-	chrX:124167136-124168758	eGFP control	eGFP-hTLX	0	0.640327		5.00E-05	0.026291

Note. Differential expression was performed for eGFP-hTLX cells relative to the eGFP control (*P* adjusted value < .05).

Abbreviation: FPKM, fragments per kilobase of transcript per million mapped reads.

TABLE 2 Ingenuity pathway analysis (IPA) for *TLX*-overexpressed cells

	Name	Molecule Type	*P* value	Genes Identified in Current Dataset
Canonical pathways	Gustation pathway		5.47E-03	*PDE2A*, *SCNN1A*
	tRNA splicing		3.42E-02	*PDE2A*
	tRNA charging		3.51E-02	*NARS*
	Molecular mechanisms of cancer		4.59E-02	*BMP3*, *PMAIP1*
	Chemokine signaling		6.20E-02	*CXCL12*
Molecular and cellular functions	Cell death and survival		4.50E-02-1.24E-05	*CXCL12*, *PMAIP1*, *SLC7A11*, *ADGRG1*
	Carbohydrate metabolism		3.42E-02-4.32E-04	*CXCL12*, *ESRRG*, *SEPP1*
	Cellular function and maintenance		4.59E-02-4.32E-04	*CXCL12*, *ESRRG*, *DOCK2*, *PDE2A*, *PMAIP1*, *LMAN1*
	Cellular movement		4.77E-02-6.35E-04	*CXCL12*, *NARS*, *DOCK2*, *SCNN1A*, *PDE2A*
	Cell cycle		2.81E-03-9.38E-04	*CXCL12*, *TXNIP*, *ESRRG*
Upstream regulators	EHMT2	Transcription regulator	5.54E-05	*CXCL12*,*PMAIP1*
	NFYA	Transcription regulator	1.63E-04	*LMAN1*,*PMAIP1*
	NRXN1	Transporter	3.27E-04	*CXCL12*,*PCDH19*
	RUNX1	Transcription regulator	4.18E-04	*ADGRG1*,*PMAIP1*
	AR	Ligand-dependent nuclear receptor	4.49E-04	*CXCL12*,*LMAN1*,*SLC7A11*
	PDX1	Transcription regulator	4.67E-04	*PMAIP1*,*TXNIP*
	MLXIP	Other	8.70E-04	*TXNIP*
	SCNN1G	Ion channel	8.70E-04	*SCNN1A*
	NEDD4L	Enzyme	8.70E-04	*SCNN1A*
	PI3K (family)	Group	1.67E-03	*CXCL12*,*TXNIP*
Networks	Cellular development, cellular growth and proliferation, cancer			*ESRRG*, *GAPDH*, *CDKN1B*, *TXNIP*, *SLC7A11*, *LMAN1*, *PKM*, *CDKN1A*, *BCAS2*, *ELMO1*, *DOCK2*, *AR*, *FOXO1*, *PMAIP1*, *ZBTB17*, *ERG*, *IGF2R*, *JMJD1C*, *TNF*, *SGK1*, *SEPP1*, *SCNN1A*, *ADGRG1*, *GDF2*, *EPHB2*, *mir-24*, *NLRP12*, *IL1B*, *G-protein-beta*, *CXCL12*, *miR-24-3p*, *LOXL2*, *estrogen receptor*, *PCDH19*, *CCR2*
	Amino acid metabolism, nucleic acid metabolism, small molecule biochemistry			*NARS*, *MAT2B*
	Cell-to-cell signaling and interaction, cancer, gastrointestinal disease			*PDE2A*, *KIAA1524*, *NONO*

Note. Statistically significant canonical pathways, molecular and cellular functions, upstream regulators, and networks were determined using ingenuity pathway analysis with Fisher's exact test (*P* value < .05). Red and green indicate upregulation and downregulation, respectively, in eGFP-hTLX cells compared with the eGFP control.

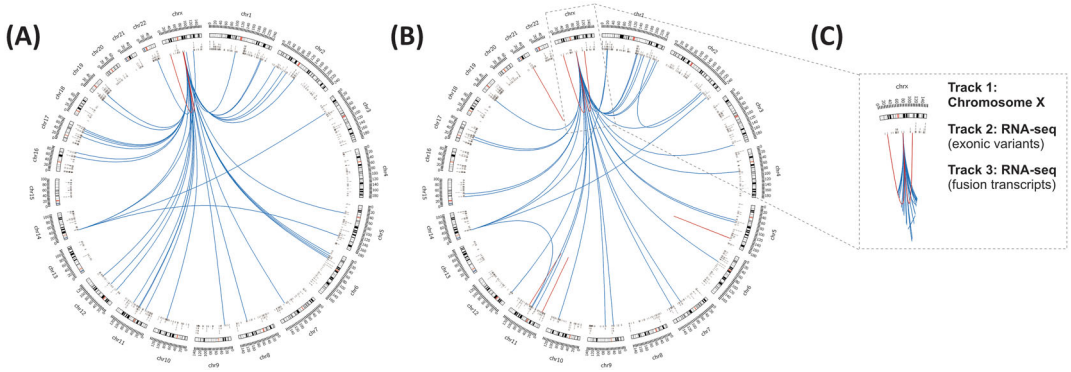

FIGURE 4 Genomic rearrangements and exonic variants in eGFP control and eGFP-hTLX HEK 293T cells. A-B, Circos plots illustrating genomic rearrangements (interchromosomal and intrachromosomal fusions) and exonic variants in eGFP control and eGFP-hTLX HEK 293T cells. Exonic variants are displayed as vertical gray lines and interchromosomal and interchromosomal fusions are displayed as dark blue and dark red lines, respectively. C Each circle from the periphery to the core represents the following: Chromosomal location, exonic variants, and gene fusions

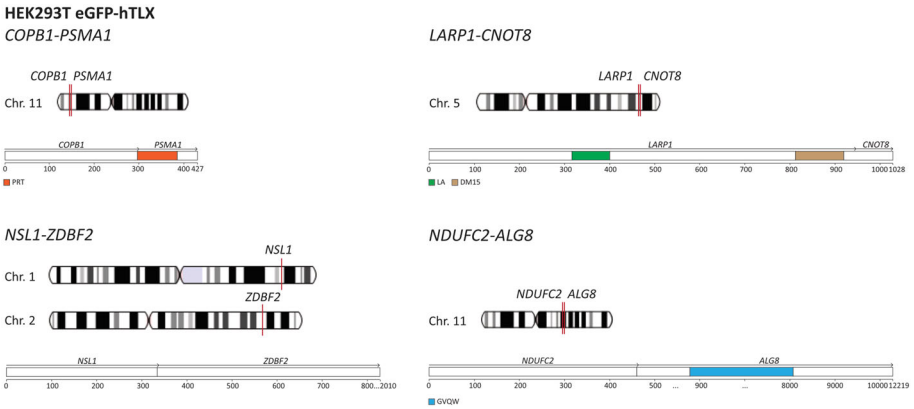

FIGURE 5 Overview of gene fusions with potential functional activity in *TLX*-overexpressing cells. Schematic overview of the chromosomal position of the fusion genes (top) and the retained protein domains (bottom). No functional domains were retained in the *NSL1-ZDBF2* gene fusion. Illustrated protein domains: PRT, proteasome domain; LA, La domain; DM15, DM15 domain; GVQW, GVQW domain

Exome Sequencing Project databases. In total, 22 070 (eGFP) and 31 460 (eGFP-hTLX) genomic and 516 (eGFP) and 520 (eGFP-hTLX) exonic regions were identified. Genetic variants in intergenic, intronic, and ncRNA intronic regions were more prevalent in *TLX*-overexpressing cells. No distinct differences in the number of exonic variants were found between *TLX*-overexpressing and control cells. In both cell lines, the majority of genetic variants were found in intergenic and intronic regions in the genome, as well as, nonsynonymous and synonymous SNVs in exonic regions. Base-pair substitutions were most commonly identified in T>C and A>G (genome) and C>T, T>C, G>A, and A>G (exon). Relative to eGFP cells, *TLX*-overexpressing cells contained 441 unique exonic variants, of which 125 variants spanning 124 unique genes were characterized as potentially deleterious (frameshift insertion (n = 58), frameshift deletion (n = 58), or stopgain (*n* = 9); Table S2). Eleven of the 125 potentially deleterious genetic variants (frameshift deletion in *FHIT*, *LRRIQ1*, *N4BP2L1*, *SND1*, *ZNF418*; frameshift insertion in *SDR16C5*, *SEC63*, *SECISBP2*, *ZNF165*; stopgain in *CRYBG1* and *TECPR1*) were found to have at least 1.5-fold change in gene expression (downregulation/frameshift deletion or upregulation/frameshift insertion and stopgain) in *TLX*-overexpressing cells compared with controls. Intriguingly, five of the 11 variants (*FHIT*, *LRRIQ1*, *N4BP2L1*, *SEC63*, and *CRYBG1*) span common fragile sites in the human genome and none of the 11 variants have been previously reported in the COSMIC database.

4 | DISCUSSION

Orphan NR TLX is a transcription factor that controls neurogenesis and NSC self-renewal and has recently been implicated in cancer where elevated TLX expression is associated with aggressive tumor features and unfavorable patient prognosis. Here, we describe genetic, transcriptomic, and phenotypic modulations in HEK 293T cells following *TLX* overexpression. We show that *TLX*-overexpressing cells exhibit chromosomal instability and oncogenic properties.

The HEK 293 cell line and its derivatives (ie, 293S, 293SG, 293SGGD, 293FTM, and 293T) are genomically instable embryonic cells that originate from adrenal precursor structures.[46] Genotoxic stresses such as transgene overexpression can induce chromosomal instability and phenotypic changes that are unrelated to the gene of interest. This phenomenon is common in HEK 293 cell lines, particularly HEK 293T cells that are inherently unstable due to overexpression of the SV40 T antigen that binds and inactivates[46,47] *p53*.

However, use of the cadmium chloride inducible vector system allowed us to monitor genotypic and phenotypic changes associated with the transfection process. We were therefore able to demonstrate that isochromosome i(6q) formed after transfection with the eGFP-hTLX vector. However, expression analysis highlighted that although noninduced eGFP-hTLX cells showed elevated *TLX* expression due to an increase in DNA copy number (via isochromosome formation), *TLX* expression was 3.6-fold higher in response to cadmium chloride treatment. According to the Mitelman database of Chromosome Aberrations and Gene Fusions in Cancer, isochromosomes on the long arm of chromosome 6 are relatively rare in cancer, with only eight reported cases. Isochromosome formation is proposed to occur when telomere attrition on one chromosome leads to reacquisition of the telomere from a donor chromosome, initiating a cascade of breakage-fusion-bridge cycles and chromosome instability on the donor chromosome.[48]

TLX plays a pivotal role in the proliferation of NSCs with deletions in *p21*, *p53*, and/or *Pten* and the formation of NSC-derived gliomas.[33,49] In the present study, we show evidence of disruption to cell cycle progression due to G0-G1 arrest and repression of *CDKN1A*/p21 and *PTEN* activity following isochromosome formation (noninduced eGFP-*hTLX*) and *TLX* overexpression (induced eGFP-*hTLX*). GO analysis using transcriptomic data revealed an association between *TLX* overexpression in HEK 293T cells and the CNS, senescence, cellular growth and proliferation, and cancer-related processes. These results are in line with our recent studies in neuroblastoma and glioblastoma showing an association between TLX knockdown and a reduction in tumorsphere formation, migratory and invasive properties, and TGFβ signaling.[22,25,29] Conversely, TLX was found to be elevated in neuroblastomas, mediated proliferation, and sphere-forming capabilities in neuroblastoma cell populations and was a predictor of adverse clinical outcome in patients with neuroblastoma.[22,29] Interestingly, several NRs were identified as upstream regulators in *TLX*-overexpressing cells, ie, AR, ESR1, ESR2, NR1H4, and NR3C2. These findings further illustrate potential crosstalk between different NRs, as previously demonstrated between TLX, AR, and ERα in breast and prostate cancer.[24,26,28,30] Gao and colleagues recently showed that although gene fusions are rarely the sole driver of carcinogenesis (approximately 1% of cancer cases), driver fusions are responsible for the development of about 16% of cancer cases.[50] Here, further analysis of the RNA-seq data for *TLX*-overexpressing cells identified two cancer-driving fusion genes (*LARP1-CNOT8* and *NSL1-ZDBF2*) and four putative deleterious genetic variants (frameshift insertions in the *CTSH*, *DBF4*, *POSTN*, and *WDR78* genes) previously found in cancers of the large intestine, breast and ovary (COSMIC database). Intriguingly, none of these genetic features were found in wild type or eGFP control samples.

In summary, our findings not only reveal cancer-related molecular features associated with *TLX* overexpression in HEK 293T cells but also provide insight into potential crosstalk between TLX and other NRs. Our work may therefore provide a basis for future studies investigating TLX in cancer, thereby identifying potential therapeutic targets for individualized treatment.

AVAILABILITY OF DATA AND MATERIAL

The RNA-seq data are accessible through the National Center for Biotechnology Information (NCBI) Gene Expression Omnibus (GEO accession GSE120893; http://www.ncbi.nlm.nih.gov/geo/query/acc.cgi?acc=GSE120893).

ACKNOWLEDGEMENTS

We are grateful to Professor P. Meraldi and Professor S. Souchelnytskyi for generously providing the HEK 293T cell line and the pMEP inducible vector.

AUTHORS' CONTRIBUTIONS

All authors had full access to the data in the study and take responsibility for the integrity of the data and the accuracy of the data analysis. *Conceptualization*, K.F.; *Methodology*, T.Z.P., D.V.-H., S.S., and K.F.; *Investigation*, T.Z.P., D.V.-H., and S.S.; *Formal Analysis*, T.Z.P.; *Writing—Original draft*, T.Z.P. and K.F.; *Writing—Review & Editing*, T.Z.P., D.V.-H., S.S., and K.F.; *Funding Acquisition*, K. F and D.V.-H.; *Visualization*, T.Z.P. and D.V.-H.; *Supervision*, K.F.

FUNDING INFORMATION

This work was supported by grants from the Swedish Childhood Cancer Fund (Grant numbers 09/001, PROJ07/003 and NBCNSPDHEL11/002), ALF (Västra Götaland Region, Sahlgrenska University Hospital; Grant number 76420), the Swedish Research Council (Grant numbers 2010/2628 and 521-2007-2098), the Swedish Cancer Society (Grant numbers 12/386, 09/0669 and 07/0081), and Assar Gabrielsson Research Foundation for Clinical Cancer Research (Grant number FB12-94). The funders had no role in study design, data collection and analysis, decision to publish, or preparation of the manuscript.

CONFLICT INTEREST

The authors declare that they have no competing interests.

ORCID

Toshima Z. Parris https://orcid.org/0000-0003-0834-5540

REFERENCES

1. Dhiman VK, Bolt MJ, White KP. Nuclear receptors in cancer—uncovering new and evolving roles through genomic analysis. *Nat Rev Genet*. 2018;19(3):160-174.
2. Robinson-Rechavi M, Carpentier AS, Duffraisse M, Laudet V. How many nuclear hormone receptors are there in the human genome? *Trends Genet*. 2001;17(10):554-556.
3. Monaghan AP, Grau E, Bock D, Schutz G. The mouse homolog of the orphan nuclear receptor tailless is expressed in the developing forebrain. *Development*. 1995;121(3):839-853.

4. Yu RT, McKeown M, Evans RM, Umesono K. Relationship between Drosophila gap gene tailless and a vertebrate nuclear receptor Tlx. *Nature*. 1994;370(6488):375-379.

5. Miyawaki T, Uemura A, Dezawa M, et al. Tlx, an orphan nuclear receptor, regulates cell numbers and astrocyte development in the developing retina. *The Journal of Neuroscience: The Official Journal of the Society for Neuroscience*. 2004;24(37):8124-8134.

6. Uemura A, Kusuhara S, Wiegand SJ, Yu RT, Nishikawa S. Tlx acts as a proangiogenic switch by regulating extracellular assembly of fibronectin matrices in retinal astrocytes. *J Clin Invest*. 2006;116(2):369-377.

7. Young KA, Berry ML, Mahaffey CL, et al. Fierce: a new mouse deletion of Nr2e1; violent behaviour and ocular abnormalities are background-dependent. *Behav Brain Res*. 2002;132(2):145-158.

8. Groszer M, Erickson R, Scripture-Adams DD, et al. PTEN negatively regulates neural stem cell self-renewal by modulating G0-G1 cell cycle entry. *Proc Natl Acad Sci U S a*. 2006;103(1):111-116.

9. Groszer M, Erickson R, Scripture-Adams DD, et al. Negative regulation of neural stem/progenitor cell proliferation by the Pten tumor suppressor gene in vivo. *Science (New York, NY)*. 2001;294(5549):2186-2189.

10. Liu HK, Belz T, Bock D, et al. The nuclear receptor tailless is required for neurogenesis in the adult subventricular zone. *Genes Dev*. 2008;22(18):2473-2478.

11. Sun G, Yu RT, Evans RM, Shi Y. Orphan nuclear receptor TLX recruits histone deacetylases to repress transcription and regulate neural stem cell proliferation. *Proc Natl Acad Sci U S a*. 2007;104(39):15282-15287.

12. Qu Q, Sun G, Li W, et al. Orphan nuclear receptor TLX activates Wnt/beta-catenin signalling to stimulate neural stem cell proliferation and self-renewal. *Nature cell biology*. 2010;12(1):31-40. sup pp 1–9

13. Zhang CL, Zou Y, He W, Gage FH, Evans RM. A role for adult TLX-positive neural stem cells in learning and behaviour. *Nature*. 2008;451(7181):1004-1007.

14. Urban N, Guillemot F. Neurogenesis in the embryonic and adult brain: same regulators, different roles. *Front Cell Neurosci*. 2014;8:396.

15. Zhang CL, Zou Y, Yu RT, Gage FH, Evans RM. Nuclear receptor TLX prevents retinal dystrophy and recruits the corepressor atrophin1. *Genes Dev*. 2006;20(10):1308-1320.

16. Liu HK, Wang Y, Belz T, et al. The nuclear receptor tailless induces long-term neural stem cell expansion and brain tumor initiation. *Genes Dev*. 2010;24(7):683-695.

17. Li W, Sun G, Yang S, et al. Regulates cell cycle progression in neural stem cells of the developing brain. *Molecular endocrinology (Baltimore, Md)*. 2008;22(1):56-64.

18. Shi Y, Chichung Lie D, Taupin P, et al. Expression and function of orphan nuclear receptor TLX in adult neural stem cells. *Nature*. 2004;427(6969):78-83.

19. Gui H, Li S, Matise MP. A cell-autonomous requirement for Cip/Kip cyclin-kinase inhibitors in regulating neuronal cell cycle exit but not differentiation in the developing spinal cord. *Dev Biol*. 2007;301(1):14-26.

20. Iwahara N, Hisahara S, Hayashi T, Horio Y. Transcriptional activation of NAD+-dependent protein deacetylase SIRT1 by nuclear receptor TLX. *Biochem Biophys Res Commun*. 2009;386(4):671-675.

21. Islam MM, Zhang CL. TLX: a master regulator for neural stem cell maintenance and neurogenesis. *Biochim Biophys Acta*. 2015;1849(2):210-216.

22. Chavali PL, Saini RK, Zhai Q, et al. TLX activates MMP-2, promotes self-renewal of tumor spheres in neuroblastoma and correlates with poor patient survival. *Cell Death Dis*. 2014;5:e1502.

23. Cui Q, Yang S, Ye P, et al. Downregulation of TLX induces TET3 expression and inhibits glioblastoma stem cell self-renewal and tumorigenesis. *Nat Commun*. 2016;7:10637.

24. Jia L, Wu D, Wang Y, et al. Orphan nuclear receptor TLX contributes to androgen insensitivity in castration-resistant prostate cancer via its repression of androgen receptor transcription. *Oncogene*. 2018.

25. Johansson E, Zhai Q, Zeng ZJ, Yoshida T, Funa K. Nuclear receptor TLX inhibits TGF-beta signaling in glioblastoma. *Exp Cell Res*. 2016;343(2):118-125.

26. Lin ML, Patel H, Remenyi J, et al. Expression profiling of nuclear receptors in breast cancer identifies TLX as a mediator of growth and invasion in triple-negative breast cancer. *Oncotarget*. 2015;6(25):21685-21703.

27. Molloy TJ, Roepman P, Naume B, van't Veer LJ. A prognostic gene expression profile that predicts circulating tumor cell presence in breast cancer patients. *PLoS One*. 2012;7(2):e32426.

28. Park HJ, Kim JK, Jeon HM, et al. The neural stem cell fate determinant TLX promotes tumorigenesis and genesis of cells resembling glioma stem cells. *Mol Cells*. 2010;30(5):403-408.

29. Sobhan PK, Zhai Q, Green LC, Hansford LM, Funa K. ASK1 regulates the survival of neuroblastoma cells by interacting with TLX and stabilizing HIF-1alpha. *Cell Signal*. 2017;30:104-117.

30. Wang Z, Wu D, Ng CF, et al. Nuclear receptor profiling in prostatospheroids and castration-resistant prostate cancer. *Endocr Relat Cancer*. 2018;25(1):35-50.

31. Zeng ZJ, Johansson E, Hayashi A, et al. TLX controls angiogenesis through interaction with the von Hippel-Lindau protein. *Biology Open*. 2012;1(6):527-535.

32. Zhu Z, Khan MA, Weiler M, et al. Targeting self-renewal in high-grade brain tumors leads to loss of brain tumor stem cells and prolonged survival. *Cell Stem Cell*. 2014;15(2):185-198.

33. Zou Y, Niu W, Qin S, Downes M, Burns DK, Zhang CL. The nuclear receptor TLX is required for gliomagenesis within the adult neurogenic niche. *Mol Cell Biol*. 2012;32(23):4811-4820.

34. Wu D, Yu S, Jia L, et al. Orphan nuclear receptor TLX functions as a potent suppressor of oncogene-induced senescence in prostate cancer via its transcriptional co-regulation of the CDKN1A (p21(WAF1) (/) (CIP1)) and SIRT1 genes. *J Pathol*. 2015;236(1):103-115.

35. Kaluz S, Kolble K, Reid KB. Directional cloning of PCR products using exonuclease III. *Nucleic Acids Res*. 1992;20(16):4369-4370.

36. Vizlin-Hodzic D, Johansson H, Ryme J, Simonsson T, Simonsson S. SAF-A has a role in transcriptional regulation of Oct4 in ES cells through promoter binding. *Cell Reprogram*. 2011;13(1):13-27.

37. Flynn RL, Centore RC, O'Sullivan RJ, et al. TERRA and hnRNPA1 orchestrate an RPA-to-POT1 switch on telomeric single-stranded DNA. *Nature*. 2011;471(7339):532-536.

38. Yanez GH, Khan SJ, Locovei AM, Pedroso IM, Fletcher TM. DNA structure-dependent recruitment of telomeric proteins to single-stranded/double-stranded DNA junctions. *Biochem Biophys Res Commun*. 2005;328(1):49-56.

39. Helou K, Wallenius V, Qiu Y, et al. Amplification and overexpression of the hepatocyte growth factor receptor (HGFR/MET) in rat DMBA sarcomas. *Oncogene*. 1999;18(21):3226-3234.

40. Rebsamen M, Pochini L, Stasyk T, et al. SLC38A9 is a component of the lysosomal amino acid sensing machinery that controls mTORC1. *Nature*. 2015;519(7544):477-481.

41. Parris TZ, Ronnerman EW, Engqvist H, et al. Genome-wide multi-omics profiling of the 8p11-p12 amplicon in breast carcinoma. *Oncotarget*. 2018;9(35):24140-24154.

42. Lampa S, Dahlo M, Olason PI, Hagberg J, Spjuth O. Lessons learned from implementing a national infrastructure in Sweden for storage and analysis of next-generation sequencing data. *Gigascience*. 2013;2(1):9.

43. Vizlin-Hodzic D, Zhai Q, Illes S, et al. Early onset of inflammation during ontogeny of bipolar disorder: the NLRP2 inflammasome gene distinctly differentiates between patients and healthy controls in the transition between iPS cell and neural stem cell stages. *Transl Psychiatry*. 2017;7(1):e1010.

44. Gene Ontology Consortium: going forward. Nucleic Acids Res, 2015;43(Database issue):D1049-D1056.

45. Ashburner M, Ball CA, Blake JA, et al. Gene ontology: tool for the unification of biology. *The Gene Ontology Consortium Nat Genet*. 2000; 25(1):25-29.

46. Lin YC, Boone M, Meuris L, et al. Genome dynamics of the human embryonic kidney 293 lineage in response to cell biology manipulations. *Nat Commun*. 2014;5:4767.

47. Stepanenko AA, Dmitrenko VV. HEK293 in cell biology and cancer research: phenotype, karyotype, tumorigenicity, and stress-induced genome-phenotype evolution. *Gene*. 2015;569(2):182-190.

48. Sabatier L, Ricoul M, Pottier G, Murnane JP. The loss of a single telomere can result in instability of multiple chromosomes in a human tumor cell line. *Mol Cancer Res*. 2005;3(3):139-150.

49. Li GL, Fang SH, Xu B. Monitoring in real time the effect of TLX overexpression on proliferation and migration of C6 cells. *Neoplasma*. 2017;64(1):48-55.

50. Gao Q, Liang WW, Foltz SM, et al. Driver fusions and their implications in the development and treatment of human cancers. *Cell Rep*. 2018;23(1):227-238. e3

SUPPORTING INFORMATION

Additional supporting information may be found online in the Supporting Information section at the end of the article.

How to cite this article: Parris TZ, Vizlin-Hodzic D, Salmela S, Funa K. Tumorigenic effects of *TLX* overexpression in HEK 293T cells. *Cancer Reports*. 2019;2:e1204. https://doi.org/10.1002/cnr2.1204